RSC Advances

PAPER

View Article Online
View Journal | View Issue

Cite this: *RSC Adv.*, 2017, **7**, 29065

Assembly of CdS nanoparticles on boron and fluoride co-doped TiO_2 nanofilm for solar energy conversion applications†

Qi Lu,[a] Ling Li,*[a] Junying Xiao,[a] Huidong Sui,[a] Jianwei Li,[a] Ruyue Duan,[a] Jingbo Li,[a] Wenming Zhang,*[a] Xiaowei Li,[a] Kunyang,[a] Yucang Zhang*[b] and Mingxing Wu*[ac]

Received 15th March 2017
Accepted 15th May 2017

DOI: 10.1039/c7ra03071a

rsc.li/rsc-advances

A highly crystalline mesoporous boron and fluoride (B/F) co-doped TiO_2 nanomaterial is successfully synthetized using a facile process, followed by chemical bath deposition (CBD) in an organic solution to prepare the QD-cell to ensure high wettability and superior penetration ability of the B/F co-doped TiO_2 films. A modified polysulfide redox couple, $((CH_3)_4N)_2S/((CH_3)_4N)_2S_n$, was employed in a cadmium sulfide (CdS) quantum dot (QD)-sensitized B/F co-doped TiO_2 solar cell covered with ZnS passivation layers with cobalt sulfide (CoS) as a counter electrode; then, an open-circuit photovoltage of 1.223 V, a high FF of 85.9%, a short-circuit photocurrent (J_{sc}) of 4.52 mA cm^{-2}, and a high overall energy conversion of 4.74% were obtained.

1. Introduction

Quantum-dot-sensitized solar cells (QDSSCs), as a derivative of dye-sensitized solar cells (DSCs), have attracted extensive attention in recent years due to their higher theoretical conversion efficiency and lower production costs. Recently, a series of QDs (CdS, CdSe, PbS, $CdSe_xTe_{1-x}$, and $CuInS_2$) and their derivatives[1–10] were employed as light-absorber sensitizers. The metal-oxide film electrode, electrolyte as well as counter electrode were also systematically optimized to improve the performance of QDSCs[11–16] as inorganic QDs exhibit various advantages over organic dyes, such as easy obtainability, low cost, high molar extinction coefficiency and convertibility of the band gap.[17–19] More importantly, QDs can harvest hot electrons, generate multiple electron–hole pairs and be designed with intermediate bands, which offer the opportunity to achieve considerable high performance solar cells.[20] The theoretical conversion efficiency of QDSSCs is as high as 44%,[21,22] which makes the QDs prominent candidates for application in solar cells. However, the photoelectric conversion efficiency of QDSSCs is still lower than that of the DSSCs because of the severe recombination of electrons of the quantum dot conduction band. Recent advances in quantum dot solar cells (QDSCs) have propelled them to the forefront of the photovoltaic research, for power conversion efficiencies (PCEs) in excess of 11% that have been achieved by Zhong's group.[23] This is a new record efficiency for QD solar cells in any configuration and also a new record for QDSSCs with any QD sensitizer. To date, the highest reported efficiency of CdS (QDSSCs) using I^-/I_3^- based electrolyte and Pt counter electrode is 1.84%.[24]

In the past few years, there has been a considerable effort to enhance the energy conversion efficiencies of QDSSCs using various strategies. A review of the literature indicates that much of the research in QDSSCs has been focused on the synthesis of various structures of photoanodes,[25,26] sensitizing the photoanodes with various combinations of QDs,[27,28] depositing QDs on an anode with various chemical methods,[29] and changing the chemical composition of the redox electrolyte.[30–34] With an important role in QDSSCs, TiO_2 films act as the support for QD loading and charge transport medium, and thus numerous studies have been carried out to exploit efficient TiO_2 nanostructures.[35–37] Chen *et al.* fabricated a novel double-sided CdS quantum-dot-sensitized TiO_2 nanotube (TNT)/ITO photoelectrode, and the experimental results show that the double-sided CdS quantum-dot-sensitized NT/ITO photoelectrodes show enhanced light absorption and achieve an optimum conversion efficiency of 7.5%, which is an enhancement of about 120% when compared with the single-sided CdS/TNT/Ti photoelectrode.[38] In either DSCs or QDSSCs, the nanoparticle porous film electrode plays a key role in the improvement of power conversion efficiency. However, TiO_2 is a large band gap semiconductor ($E_g = 3.2$ eV), which can only be excited by UV radiation at a wavelength below 390 nm. To make better use of the full light spectrum, doping TiO_2 with metal and nonmetal elements has

[a]*Hebei Key Lab of Optic-electronic Information and Materials, College of Physics Science and Technology, Hebei University, Baoding 071002, P. R. China. E-mail: lilinghbu@163.com; wmzhang@hbu.edu.cn; Fax: +86 312 5079355; Tel: +86 312 5079355*

[b]*Key Laboratory of Ministry of Education for Advanced Materials in Tropical Island Resources in Hainan University, Haikou 570228, P. R. China. E-mail: yczhang@hainu.edu.cn*

[c]*College of Chemistry and Material Science, Hebei Normal University, No. 20 Rd. East of 2nd Ring South, Yuhua District, Shijiazhuang City, Hebei Province, 050024, P. R. China. E-mail: mingxing.wu@mail.hebtu.edu.cn*

† Electronic supplementary information (ESI) available. See DOI: 10.1039/c7ra03071a

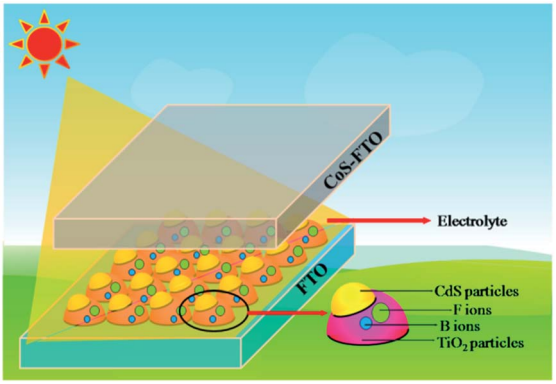

Scheme 1 Schematic of the CdS QD-sensitized B/F co-doped TiO_2 solar cell structure.

been considered as a promising way to tailor the electronic properties of TiO_2 photoanodes in QDSSCs and has succeeded in improving photovoltaic performance of QDSSCs. In particular, non-metallic doping of TiO_2 electrodes has attracted much attention due to the excellent performance of the resulting doped material. Moreover, the technology of co-doping has been proven to be an effective solution to improve the performance of the TiO_2 electrodes due to its charge compensation on the basis of different ions through an internal charge transfer, with a large stabilization effect resulting in a less defective co-doped TiO_2 system.[39,40]

To the best of our knowledge, research into non-metallic B/F co-doping in QDSSCs has not been systematically carried out. Therefore, it would be highly desirable to research the co-doping effect on QDSSC systems. Herein, we investigated the effect of B/F co-doping on the QDSSC's performance and demonstrated that the application of a B/F co-doped TiO_2 electrode in QDSSCs can enhance the photovoltaic performance of QDSSCs. In this study, we report the first example of CdS quantum dot (QD)-sensitized B/F co-doped TiO_2 solar cells with ZnS passivation layers using CoS as a counter electrode. The configuration of the cells is illustrated in Scheme 1. As a result, a CdS QD-sensitized B/F co-doped TiO_2 solar cell using the same $((CH_3)_4N)_2S/((CH_3)_4N)_2S_n$ electrolyte shows a promising photovoltaic performance, with an efficiency of 4.74%, a significantly high V_{oc} of 1.223 V, and a high FF of 85.9% with a short-circuit photocurrent (J_{sc}) of 4.52 mA cm^{-2}.

2. Experimental

2.1 Preparation of B–F co-doped TiO_2 nanoparticles

The doped and modified nanocrystalline powder was synthesized using the sol–gel route, followed by pyrolysis and calcination treatments. Titanium tetraisopropoxide (Ti(O*i*-Pr)$_4$) (Alfa Aesar), acetylacetone (acac, Aldrich), boron fluoride acetic acid complex ($BF_3 \cdot 2CH_3CO_2$, 97%), and tetrafluoroboric acid (HBF_4, 48%, Strem Chemicals, Newburyport, MA) were used as received. An alcoholic complex was prepared by slowly adding $BF_3 \cdot 2CH_3CO_2$ (0.03 mol) to 10 mL of EtOH at 0 °C under ambient conditions, which formed a homogeneous and viscous solution. Once this solution cooled to room temperature, it was slowly added to Ti(O*i*Pr)$_4$ (0.07 mol) in 10 mL *i*PrOH, producing a vivid yellow homogeneous solution. After the mixture was stirred for 15 min, deionized water (500 mL) was added, which brought no discernible change; hence 100 mL of HBF_4 was added, and after a few minutes, the yellow solution became turbid. It was then refluxed at 80 °C for 30 min, which effectively rehomogenized the mixture (pH: 1–2). After the mixture was refluxed for 6 h at 70 °C, Ti(O*i*Pr)$_4$ (0.069 mol) was added to the reaction vessel to facilitate particle formation, and refluxing was continued for 18 h at 70–80 °C while stirring. The volume of the solution was reduced to approximately one-fifth, yielding a finely dispersed white powder. The powder was separated by filtration through a medium porosity ceramic frit, repeatedly washed with water until the pH of the filtrate was neutral and finally dried at 100 °C in an oven.

The as-synthesized material was subjected to different thermal treatments. Specifically, the purified powder was placed in a borosilicate test tube, which was attached to a glass manifold employing Cajon connectors and stainless steel tubing, and was heated to 400 °C (4 °C min^{-1}). A short ceramic oven was employed to allow manipulation of the sample tube while it was still connected to the manifold. The sample's appearance was monitored visually over the course of the heating procedure, and the temperature was increased to 500 °C while under vacuum or under gas flow for periods of up to 3 h. The heavily reduced powder, on the basis of its coloration (gray), was exposed briefly to air by opening the vessel to the atmosphere or to pure oxygen gas that was delivered directly to the sample container. The final stage of the thermal treatment consisted of the evacuation of the tube's contents or rapidly cooling it to 100 °C while in air.

2.2 Deposition of CdS QD-sensitized B–F co-doped TiO_2 solar cells

The B–F co-doped TiO_2 (B–F–TiO_2) oxide used in the front subcell electrode was individually mixed with a polymer binder, and dissolved in terpineol, resulting in a paste. The paste was then coated on the fluorine-doped (FTO) S_nO_2 conductive glass (TEC15, 15 Ω per square, Pilkington, USA) by screen printing and then dried for 5 min at 125 °C. This procedure was repeated 4 times (to give *ca.* 8 μm film). The electrodes were gradually heated at 500 °C for 30 min, and the sintered film was further treated with 40 mM $TiCl_4$ aqueous solution at 70 °C for 30 min, washed with ethanol and water, and annealed at 480 °C for 30 min. SILAR was used to assemble CdS-QDs into the B–F–TiO_2 photoelectrode. B–F–TiO_2 films were surface-modified by immersing in 0.1 M mercaptoacetic acid (TGA) for 1 min; the TGA-modified B–F–TiO_2 substrate electrode was dipped first into an ethanol solution containing $Cd(NO_3)_2$ (0.5 M) for 1 min, rinsed with ethanol, and dried with an air gun. The electrodes were then dipped for another 1 min into a Na_2S methanol solution (0.5 M) and rinsed again with methanol. The process was repeated up to N cycles (N = 1 to 5). These as-prepared electrodes are represented herein as "B–F–TiO_2/TGA/CdS-N" electrodes.[41] The CdS-sensitized B–F–TiO_2 films were coated with ZnS for 3 cycles by dipping alternately into 0.1 M $Zn(OAc)_2$ methanol solution and 0.1 M Na_2S solutions for 1 min per dip. As the working electrode, CoS was separated with a hot-melt Surlyn 1702 film (25 μm, DuPont). Cleaned FTO glass was

dipped into 0.5 M $Co(NO_3)_2$ ethanolic solution for 30 s, rinsed with ethanol, and dried with an air gun. The sample was then dipped for 30 s into 0.5 M Na_2S methanolic solution, followed by rinsing with methanol and drying with an air gun. The process was repeated for up to five cycles to obtain the CoS electrode.[42] The electrolyte solution consisting of 0.01 M tetramethyl ammonium sulfide $((CH_3)_4N)_2S$, 0.002 M S, 0.02 M $LiClO_4$, 0.02 M 4-*tert*-butylpyridine (TBP), 3-methoxypropionitrile (MPN) was used as a solvent for the polysulfide electrolyte. The $((CH_3)_4N)_2S$ was prepared by heating tetramethyl ammonium hydroxide $((CH_3)_4N)OH$ and ammonium sulfide $(NH_4)_2S$ at 100 °C.[43] We investigated three experiment samples with the same conditions five times to test the repeatability and stability of the experiment, which gave excellent results.

3. Optical and photovoltaic measurements

Crystal structures of the samples were analyzed by X-ray diffraction (XRD) (Japan, XD-3A) using Cu Kα radiation and a scintillation counter detector. The patterns were recorded in the 2θ range of 20–80°. The elemental distribution and concentration were analyzed by an energy dispersive spectrometer (EDS) (Oxford Inca) attached to the field emission scanning electron microscope (FESEM). UV-vis absorption spectra were recorded on a UV-visible spectrometer (U-4100, HITACHI, Japan). The electronic structure and B–F-doping amount was determined by X-ray photoelectron spectroscopy (XPS) (AXIS-165 Shimadzu, Japan). Transmission electron microscopy (TEM) images were obtained using a JEOL JEM-2100 instrument. The flat-band potential (V_{fb}) of the nanostructured TiO_2 and B–F–TiO_2 electrode was determined by measuring the absorbance at 780 nm as a function of the applied potential. For the spectroscopic electrochemistry measurement, an 8 μm thick TiO_2 film formed the working electrode (1 cm^2 surface area) of a three-electrode photoelectrochemical cell employing a platinum wire counter electrode and an Ag/AgCl reference electrode. Potential control was carried out on a CHI 660E potentiostat, and the applied potential was scanned at 5 mV s^{-1}. A 780 nm monochromatic light source was obtained from the UV-vis spectrophotometer (U-4100, HITACHI, Japan). For each determination of V_{fb}, a new working electrode and freshly prepared electrolyte solution were used.[44]

The irradiation source for the photocurrent density–voltage (J–V) measurement was an AM 1.5G solar simulator (16S-002, SolarLight Co. Ltd., USA). The incident light intensity was 100 mW cm^{-2}, calibrated with a standard Si solar cell. The novel solar cells were masked to a working area of 0.159 cm^2. The J–V curves were obtained using a linear sweep voltammetry (LSV) method on an electrochemical workstation (LK9805, Lanlike Co. Ltd., China). The measurement of the incident photon-to-current conversion efficiency (IPCE) was performed using a Hypermonolight (SM-25, Jasco Co. Ltd., Japan) system. The short current density was calibrated by integrating the product of the IPCE value and solar photon density against the wavelength.[45] Electrochemical impedance spectroscopy (EIS) for QDSSCs under dark, with a bias of −0.75 V, was measured using an impedance/gain-phase analyzer (ZENIUM, ZAHNER, Germany). The spectral regions were scanned using a frequency range of 10^{-1} to 10^5 Hz at room temperature. The alternate current (AC) amplitude was set at 10 mV.

4. Results and discussion

4.1 Optical properties

Fig. 1 shows that the absorbance intensity of these films increases with noticeable shifts of the absorbance edge towards longer wavelength, and a shoulder to the visible light region was observed with doped B and F, where the film doped with B and F shows yellow colour while the undoped film shows white colour. The UV-vis absorption spectra of the B–F-doped TiO_2/TGA/CdS-3 film and the TiO_2/TGA/CdS-3 film in the $((CH_3)_4N)_2S/((CH_3)_4N)_2S_n$ electrolyte also shifted about 30 nm to longer wavelength, which is beneficial for for the B–F-doped TiO_2/TGA/CdS-3 film to capture more light and to obtain higher light to electrical efficiency.

4.2 Spectro-electrochemical properties

In order to further investigate the cause of the enhancement of V_{oc} in QDSSCs, the spectro-electrochemical measurements for undoped and B/F co-doped TiO_2 were carried out, and the results are shown in Fig. 2. The flat-band potential V_{fb} of TiO_2 samples with and without B/F co-doping were determined as −2.2 V and −2.097 V (*vs.* Ag/AgCl), respectively. Therefore, a higher quasi-Fermi level closer to the conduction band was definitely achieved, which could lead to the larger V_{oc} for liquid-state QDSSCs employing a B/F co-doped TiO_2 electrode.

Under Fermi level pinning, the two parameters (V_{oc} and V_{fb}) are linked by eqn (1).[46]

$$V_{oc} = |V_{fb} - V_{red}| \quad (1)$$

where V_{red} is the standard reduction potential of a redox couple, assuming that V_{red} does not vary with the addition of boron and nitrogen. Therefore, a higher quasi-Fermi level closer to the conduction band is definitely achieved, which could lead to

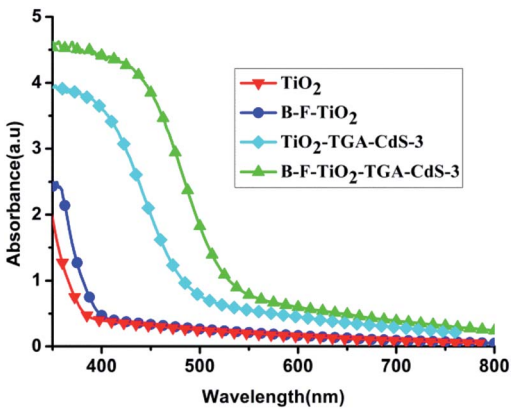

Fig. 1 UV-vis absorption spectra of the bare TiO_2 film, B–F doped TiO_2 film, TiO_2/TGA/CdS-3 film, and B–F-doped TiO_2/TGA/CdS-3 film.

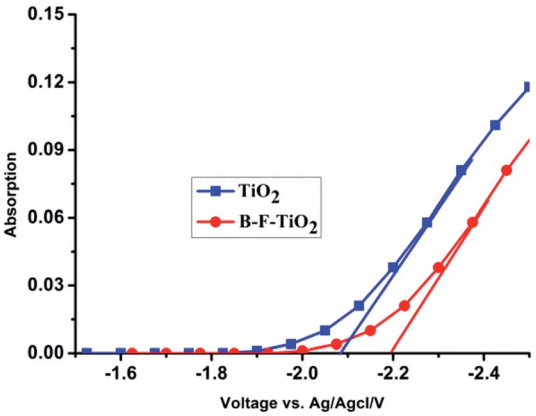

Fig. 2 Absorbance measured at 780 nm as a function of applied potential for nanostructured undoped and B/F co-doped TiO_2 electrodes at 298 K in 3 M KCl solution (Ag/AgCl reference electrode).

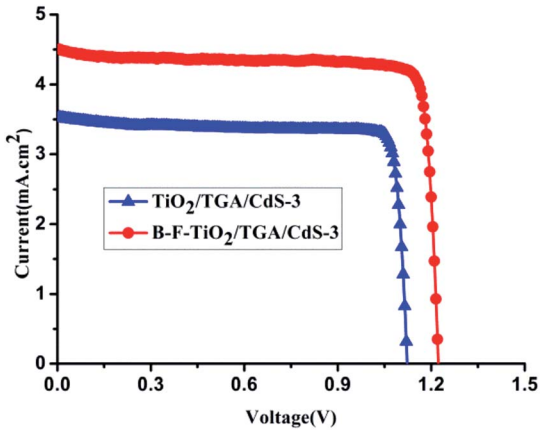

Fig. 3 The *J–V* characteristics of the B–F–TiO_2/TGA/CdS-3 cell and TiO_2/TGA/CdS-3 cell measured under illumination of 100% sun (AM 1.5, 100 mW cm^{-2}).

larger V_{oc} for liquid-state QDSSCs employing B/F co-doped TiO_2 electrodes. With the co-doping of B/F in TiO_2, its band gap was narrowed and the light capture range was significantly extended; the excellent photoelectrochemical performance could be attributed to the ideal combination of retarded electron recombination and superior energy band structure from the unique B/F co-doped TiO_2 particle structure.

4.3 Device properties

New CdS-functionalized QDSSCs were fabricated in this study in which tetramethyl ammonium sulphide/polysulfide, $((CH_3)_4N)_2S/((CH_3)_4N)_2S_n$, was used as the redox couple in an organic solvent (3-methoxy propionitrile (MPN)). The configuration of the cells is illustrated in Scheme 1.

The fill factor (FF) and the overall light-to-electrical energy conversion efficiency (η) of the DSSC were calculated according to the following equations:[47]

$$\eta(\%) = \frac{V_{max} \times J_{max}}{P_{in}} \times 100\% = \frac{V_{oc} \times J_{sc} \times FF}{P_{in}} \times 100\% \quad (2)$$

$$FF = \frac{V_{max} \times J_{max}}{V_{oc} \times J_{sc}} \quad (3)$$

where P_{in} is the incident light power, and J_{max} (mA cm^{-2}) and V_{max} (*V*) are the current density and voltage at the point of the maximum power output in the *J–V* curves, respectively.

The cell based on B–F–TiO_2/TGA/CdS-3 photoelectrode was found to give the best performance in this series. Under one sun illumination (AM 1.5G, 100 mW cm^{-2}), this cell shows an ideal energy conversion efficiency of 4.74%, a large open-circuit photovoltage of 1.223 V and an extremely high FF value up to 85.9% with a short-circuit photocurrent (J_{sc}) of 4.52 mA cm^{-2}; see Fig. 3. Compared with the cell based on TiO_2/TGA/CdS-3, the J_{sc} was improved from 3.54 mA cm^{-2} to 4.52 mA cm^{-2}, leading to an improvement in efficiencies from 3.45% to 4.74%, and the V_{oc} improved from 1.124 V to 1.223 V; the open-circuit potential of the B–F–TiO_2 electrode is negatively shifted by 99 mV compared to the undoped TiO_2 electrode, which is consistent with the flat-band potential result. Moreover, using V_{oc} as a reference is a standard way to describe the *J–V* characteristics of an electrochemical cell. V_{oc} is the light intensity dependent rest potential of the cell. Connecting the cell to an electric load causes the electric current to flow in the cell, which gives rise to voltage losses, V_k, that are also called overpotentials or overvoltages, due to the internal cell resistances R_k. This decreases the cell voltage from its open-circuit value and determines the shape of the solar cell *J–V* curve and hence its fill factor.[48]

The IPCE (incident photon-to-current conversion efficiency, also referred to as quantum efficiency) of the QDSSCs was determined by measuring the short-circuit current under incident monochromatic light irradiated through a monochromator with a grating of 1200 grooves per mm (Shimadzu Corporation, Kyoto, Japan); light from a xenon lamp passing through a monochromator (PXJ43B11-6W, Japan) was focused onto the cell. The IPCE is calculated according to the following equations:[49,50]

$$IPCE = \frac{12400 \times J_{sc}(\text{mA cm}^{-2})}{\lambda(\text{nm}) \times P_{in}(\text{mW cm}^{-2})} \quad (4)$$

where J_{sc} is the short-circuit current density (mA cm^{-2}), V_{oc} is the open-circuit voltage (*V*), P_{in} is the incident light power, and J_{max} (mA cm^{-2}) and V_{max} (*V*) are the current density and voltage in the *J–V* curves, respectively, at the point of the maximum power output.

As shown in Fig. 4, the incident photon-to-electron conversion efficiency spectrum of a B–F–TiO_2/TGA/CdS-*N* based cell is about 80% in comparison with the TiO_2/TGA/CdS-3 based cell, which is over 60% at 400 nm; therefore, the higher IPCE for the QDSC with the B–F–TiO_2/TGA/CdS-*N* electrode than that with the TiO_2/TGA/CdS-3 electrode is due to the B–F doping in the former, and the IPCE response in the visible region is in agreement with the trend for the J_{sc}. The active range in the visible light region is consistent with the corresponding UV-vis spectrum. The absorption edge of the B–F–TiO_2/TGA/CdS-3-based cell shifts towards longer wavelength of about 30 nm compared to that of TiO_2/TGA/CdS-3 based cell.

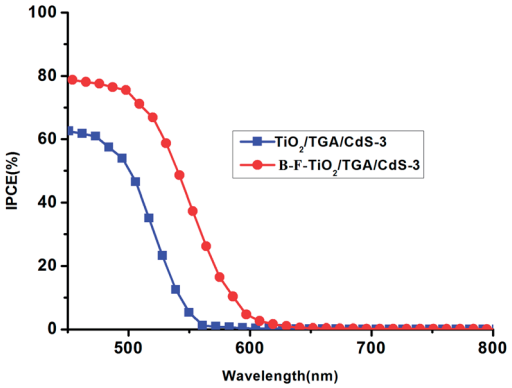

Fig. 4 The incident photon-to-current conversion efficiency (IPCE) of the cell based on TiO_2/TGA/CdS-3 electrode and B–F–TiO_2/TGA/CdS-3 electrode.

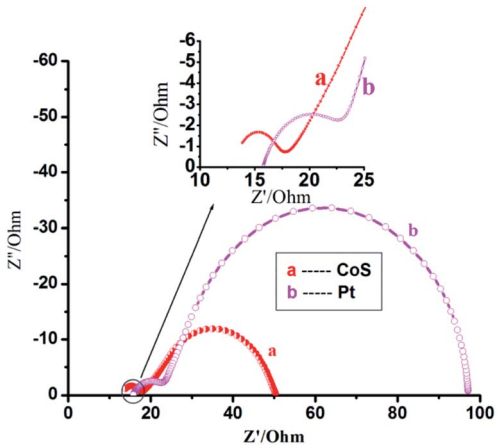

Fig. 5 Electrochemical impedance spectra for CoS and Pt counter electrodes with the same B–F–TiO_2/TGA/CdS-3 film, scanned from 10^{-1} to 10^5 Hz at room temperature. The cells were measured at −0.75 V in the dark. The alternate current (AC) amplitude was set at 10 mV.

4.4 Electrochemical impedance spectra

Fig. 5 shows the electrochemical impedance spectra[51–54] for CoS and Pt counter electrodes with the same B–F–TiO_2/TGA/CdS-3 film under forward bias (−0.75 V) in the dark. Using the identical electrolyte, the reduction rate is primarily determined by the catalytic activity of the counter electrodes. The cells for EIS measurements are symmetric thin-layer sandwich cells. At high frequency (>10^5 Hz), the ohmic series resistance (R_s) of the FTO layer, the CoS (or Pt) layer and the electrolyte can be determined in the middle frequency range of 10^{-1} to 10^5 Hz. In the low-frequency range of 0.1–10 Hz, the Warburg diffusion impedance, within the electrolyte, will be estimated. The R_s value being 3.325 Ohm for the CoS electrode is lower than the 7.583 Ohm for the Pt electrode.

5. Conclusions

In summary, we have successfully developed the first example of an efficient CdS QD-sensitized B/F co-doped TiO_2 solar cell with a modified polysulfide electrolyte in a pure organic system. B/F doping into the TiO_2 lattice results in a red shift of the electronic absorption and enhanced photocurrent response. As a result, the performance of the cell is superb with an efficiency of 4.74%, a significantly high V_{oc} of 1.223 V, and a high FF of 85.9% with a short-circuit photocurrent (J_{sc}) of 4.52 mA cm^{-2}. The results show that the combination of B/F co-doped and CdS QD sensitization of the TiO_2 thin films is an effective way to enhance the photoresponse, which is promising for photovoltaic and photoelectrochemical applications.

Acknowledgements

We gratefully acknowledge the financial support from the following sources: the National Natural Science Foundation of China (NSFC) (Grants 21201053, 11104058, 51607054), the Fund in Hebei Province Natural Science (F2014201078, A2015201050), the Youth Fund in Hebei Province Department of Education China (QN2014057, ZD2016055, ZD2015044), the College students' innovative entrepreneurial training program in Hebei Province (201610075066, 2016105, 2016127, 2016170, 2016177), the Hebei university laboratory open project (sy201639), the Outstanding Youth Fund of Hebei University (2015JQ02), the Hebei province Outstanding Youth Fund (A2017201082), The Second Batch of Young Talent of Hebei Province, and the Graduate students' innovative supporting program in Hebei university (X201730)

Notes and references

1 W. T. Sun, Y. Yu, H. Y. Pan, X. F. Gao, Q. Chen and L. M. Peng, *J. Am. Chem. Soc.*, 2008, **130**, 1124–1125.
2 L. M. Peter, D. J. Riley, E. J. Tull and K. G. U. Wijayantha, *Chem. Commun.*, 2002, **10**, 1030–1031.
3 Y. Tachibana, K. Umekita, Y. Otsuka and S. Kuwabata, *J. Phys. D: Appl. Phys.*, 2008, **41**, 102002.
4 H. Zhang, K. Cheng, Y. M. Hou, Z. Fang, Z. X. Pan, W. J. Wu, J. L. Hua and X. H Zhong, *Chem. Commun.*, 2012, **48**, 11235–11237.
5 H. C. Leventis, F. O'Mahony, J. Akhtar, M. Afzaal, P. O'Brien and S. A. Haque, *J. Am. Chem. Soc.*, 2010, **132**, 2743–2750.
6 A. Braga, S. Giménez, I. Concina, A. Vomiero and I. Mora-Seró, *J. Phys. Chem. Lett.*, 2011, **2**, 454–460.
7 Z. Pan, K. Zhao, J. Wang, H. Zhang, Y. Feng and X. Zhong, *ACS Nano*, 2013, **7**, 5215–5222.
8 P. K. Santra, P. V. Nair, K. George Thomas and P. V. Kamat, *J. Phys. Chem. Lett.*, 2013, **4**, 722–729.
9 Z. Pan, I. Mora-Seró, Q. Shen, H. Zhang, Y. Li, K. Zhao, J. Wang, X. Zhong and J. Bisquert, *J. Am. Chem. Soc.*, 2014, **136**, 9203–9210.
10 T. L. Li, Y. L. Lee and H. Teng, *Energy Environ. Sci.*, 2012, **5**, 5315–5324.
11 Z. Du, H. Zhang, H. Bao and X. Zhong, *J. Mater. Chem. A*, 2014, **2**, 13033–13040.
12 M. Hossain, J. Jennings, Z. Koh and Q. Wang, *ACS Nano*, 2011, **5**, 3172–3181.

13 K. Zhao, H. Yu, H. Zhang and X. Zhong, *J. Phys. Chem. C*, 2014, **118**, 5683–5690.
14 J. Jin, X. Zhang and T. He, *J. Phys. Chem. C*, 2014, **118**, 24877–24883.
15 Y. Jiang, B. Yu, J. Liu, Z. Li, J. Sun, X. Zhong, J. Hu, W. Song and L. Wan, *Nano Lett.*, 2015, **15**, 3088–3095.
16 N. S. Makarov, H. McDaniel, N. Fuke, I. Robel and V. I. Klimov, *J. Phys. Chem. Lett.*, 2014, **5**, 111–118.
17 H. Chen, W. Y. Fu, H. B. Yang, P. Sun, Y. Y. Zhang, L. R. Wang, W. Y. Zhao, X. M. Zhou, H. Zhao, Q. A. Jing, X. F. Qi and Y. X. Li, *Electrochim. Acta*, 2010, **56**, 919–924.
18 S. L. Cheng, W. Y. Fu, B. Y. Hai, L. N. Zhang, J. W. Ma, H. Zhao, M. L. Sun and L. H. Yang, *J. Phys. Chem. C*, 2011, **116**, 2615–2621.
19 H. M. Chen, C. K. Chen, Y. C. Chang, C. W. Tsai, R. S. Liu, S. F. Hu, W. S. Chang and K. H. Chen, *Angew. Chem., Int. Ed.*, 2010, **112**, 6102–6105.
20 J. J. Tian, Q. F. Zhang, L. L. Zhang, R. Gao, L. F. Shen, S. G. Zhang, X. H. Qu and G. Z. Cao, *Nanoscale*, 2013, **5**, 936–943.
21 Y. Qiu, S. Lu, S. Wang, X. Zhang, S. He and T. He, *J. Power Sources*, 2013, **253**, 300–304.
22 M. Deng, Q. Zhang, S. Huang, D. Li, Y. Luo, Q. Shen, T. Toyoda and Q. Meng, *Nanoscale Res. Lett.*, 2010, **5**, 986–990.
23 J. Du, Z. L. Du, J. S. Hu, Z. X. Pan, Q. Shen, J. K. Sun, D. H. Long, H. Dong, L. Sun, X. H. Zhong and L. J. Wan, *J. Am. Chem. Soc.*, 2016, **138**(12), 4201.
24 C. H. Chang and Y. L. Lee, *Appl. Phys. Lett.*, 2007, **91**, 053503.
25 H. Wang, Y. S. Bai, H. Zhang, Z. H. Zhang, J. H. Li and L. Guo, *J. Phys. Chem. C*, 2010, **114**, 16451–16455.
26 Q. Zhang, X. Guo, X. Huang, S. Huang, D. Li, Y. Luo, Q. Shen, T. Toyoda and Q. Meng, *Phys. Chem. Chem. Phys.*, 2011, **13**, 4659–4667.
27 Y. L. Lee and C. H. Chang, *J. Power Sources*, 2008, **185**, 584–588.
28 L. W. Chong, H. T. Chien and Y. L. Lee, *J. Power Sources*, 2010, **195**, 5109–5113.
29 V. Gonzalez-Pedro, C. Sima, G. Marzari, P. P. Boix, S. Gimenez, Q. Shen, T. Dittrich and I. Mora-Seró, *Phys. Chem. Chem. Phys.*, 2013, **15**, 13835–13842.
30 H. Wang, T. Kubo, J. Nakazaki, T. Kinoshita and H. Segawa, *J. Phys. Chem. Lett.*, 2013, **4**, 2455–2460.
31 Y. Li, L. Wei, R. Zhang, Y. Chen, L. Mei and J. Jiao, *Nanoscale Res. Lett.*, 2013, **8**, 89–96.
32 T. Shu, P. Xiang, Z. M. Zhou, H. Wang, G. H. Liu, H. W. Hanand and Y. D. Zhao, *Electrochim. Acta*, 2012, **68**, 166–171.
33 J. T. Xi, Q. F. Zhang, K. Park, Y. M. Sun and G. Z. Cao, *Electrochim. Acta*, 2011, **56**, 1960–1966.
34 Z. Pan, H. Zhang, K. Cheng, Y. Hou, J. Hua and X. Zhong, *ACS Nano*, 2012, **48**, 11235–11237.
35 K. Zidek, K. Zheng, C. S. Ponseca, M. E. Messing Jr, L. R. Wallenberg, P. Chabera, M. Abdellah, V. Sundstrom and T. Pullerits, *J. Am. Chem. Soc.*, 2012, **134**, 12110–12117.
36 C. W. Kung, H. W. Chen, C. Y. Lin, K. C. Huang, R. Vittal and K. C. Ho, *ACS Nano*, 2012, **214**, 91–99.
37 M. H. Deng, S. Q. Huang, Q. X. Zhang, D. M. Li, Y. H. Luo, Q. Shen, T. Toyoda and Q. B. Meng, *Chem. Lett.*, 2010, **5**, 986–990.
38 C. Chen, F. M. Li, G. Q. Li, F. R. Tan, S. J. Li and L. Y. Ling, *J. Mater. Sci.*, 2014, **49**, 1868–1874.
39 H. Xu and L. Z. Zhang, *J. Phys. Chem. C*, 2010, **114**, 11534–11541.
40 H. J. Tian, L. H. Hu, W. X. Li, J. Sheng, S. Y. Xu and S. Y. Dai, *J. Mater. Chem.*, 2011, **21**, 7074–7077.
41 R. Plass, S. Pelet, J. Kruger, M. Grätzel and U. Bach, *J. Phys. Chem. B*, 2002, **106**, 7578–7580.
42 M. Adachi, M. Sakamoto, J. Jiu, Y. Ogata and S. Isoda, *J. Phys. Chem. B*, 2006, **110**, 13872–13880.
43 L. Li, X. C. Yang, J. J. Gao, J. Z. Zhao and A. Hagfeldt, *J. Am. Chem. Soc.*, 2011, **133**, 8458–8460.
44 H. J. Tian, L. H. Hu, C. N. Zhang, W. Q. Liu, Y. Huang, L. Mo, L. Guo, J. Sheng and S. Y. Dai, *J. Phys. Chem. C*, 2010, **114**, 1627–1632.
45 G. Liu, Y. N. Zhao, C. H. Li, F. Sun, G. Q. Lu and H. M. Cheng, *Angew. Chem., Int. Ed.*, 2008, **47**, 5416–4520.
46 T. S. Kang, K. H. Chun, J. S. Hong, S. H. Moon and K. Kim, *J. Electrochem. Soc.*, 2000, **147**, 3049–3053.
47 M. Grätzel, *Prog. Photovoltaics*, 2000, **8**, 171–185.
48 J. Halme, P. Vahermaa, K. Miettunen and P. Lund, *Adv. Mater.*, 2010, **22**, 210–234.
49 M. K. Nazeeruddin, P. Péchy, T. Renouard, S. M. Zakeeruddin, R. H. Baker, P. Comte, P. Liska, L. Cevey, E. Costa, V. Shklover, L. Spiccia, G. B. Deacon, C. A. Bignozzi and M. Grätzel, *J. Am. Chem. Soc.*, 2001, **123**, 1613–1624.
50 T. Renouard, R. Fallahpour, M. K. Nazeeruddin, R. Humphry-Baker, S. Gorelsky, A. Lever and M. Grätzel, *Inorg. Chem.*, 2002, **41**, 367–373.
51 M. Adachi, M. Sakamoto, J. Jiu, Y. Ogata and S. Isoda, *J. Phys. Chem. B*, 2006, **110**, 13872–13880.
52 Q. Wang, J. Moser and M. Grätzel, *J. Phys. Chem. B*, 2005, **109**, 14945–14953.
53 Z. S. Wang, N. Cui, Y. Koumura, M. Takahashi, H. Sekiguchi, A. Mori, T. Kubo, A. Furube and K. Hara, *Chem. Mater.*, 2008, **20**, 3993–4003.
54 X. Y. Yu, J. Y. Liao, K. Q. Qiu, D. B. Kuang and C. Y. Su, *ACS Nano*, 2011, **5**, 9494–9500.

